minerals

MDPI

Article

Ceramic Materials Based on Clay and Soapstone Waste: Thermo-Mechanical Properties and Application

Vera Ilyina *, Ekaterina Klimovskaya * and Tatiana Bubnova

Institute of Geology, Karelian Research Centre, Russian Academy of Sciences (IG KarRC RAS), 185910 Petrozavodsk, Russia; bubnova@krc.karelia.ru

* Correspondence: ivp@krc.karelia.ru (V.I.); klimeee@gmail.com (E.K.); Tel.: +7-(8142)-76-61-73 (V.I.)

Abstract: In order to assess the feasibility of utilizing soapstone waste, which is generated during the production of stone blocks for fireplaces and other energy-saving devices, the effect of its addition to clay on the technological and thermal properties of ceramic materials was investigated. Two local clays and soapstone processing waste were characterized using XRD, SEM-EDS, XRF, DTA-TG, and granulometric analysis. The linear firing shrinkage, water absorption, density, flexural strength, thermal conductivity, specific heat capacity, and thermal shock resistance of the fired ceramic samples were analyzed. The results have shown that addition of soapstone waste to clay in an amount of 40 wt.% increases flexural strength, enhances thermal stability, and, additionally, reduces the thermal conductivity of the experimental samples. The technological properties of the final product meet the standard requirements for ceramic tiles.

Keywords: clay; soapstone waste; ceramics; firing; flexural strength; thermal conductivity

1. Introduction

Soapstone has gained recognition worldwide as a unique natural material for thermal insulation. It is extensively used by leading Finnish companies such as Tulikivi and Nunna Uuni Oy for the production of fireplaces, stoves, and other energy-saving devices [1–3]. Soapstone is a rock containing 35–75 vol.% talc [4], formed due to metamorphism and alteration of ultramafic and magnesium carbonate rocks under low-grade conditions. In addition to talc, soapstone can include other magnesium-rich minerals such as carbonate, chlorite, serpentine, amphibole, olivine, as well as ore minerals and quartz. Along with soapstone, the term talcite refers to metamorphic rock comprising at least 75 vol.% talc. A massive variety of talcite is named steatite [5]. Soapstone deposits are being developed in various parts of the world, including Russia, Finland, Norway, Brazil, India, Canada, and the United States.

The main areas of application for talc raw material to a large extent depend on the origin of the deposits. Modern global talc production is mainly based on low-iron carbonate-derived deposits, which yield talc products with high whiteness exceeding 90% [5,6]. This high-quality talc and microtalc cover the majority of consumption in the paper, paint, and ceramic industries [7]. The mineralogy of ultramafic-hosted soapstone limits its usability for talc extraction and does not favor the production of the finest-quality high-brightness talc products (Fe_2O_3, FeO, Al_2O_3, and CaO are the principal impurity oxides). The processing of such soapstone to obtain talc concentrate involves the use of high-tech beneficiation technologies, allowing for the production of various grades of commercial talc that successfully compete in the global market (whiteness is in the range from 75% to 90%) [3,7–11]. Ferroan magnesite obtained as a byproduct of talc production from soapstones (e.g., in Finland, Norway, and Russia [8,12,13]) is of potential economic interest. Magnesite is considered as an important potential source of magnesia, which is used in a wide range of strategic industries, such as chemical, metallic, agriculture, environment, and refractory [14–16].

Citation: Ilyina, V.; Klimovskaya, E.; Bubnova, T. Ceramic Materials Based on Clay and Soapstone Waste: Thermo-Mechanical Properties and Application. *Minerals* **2023**, *13*, 1376. https://doi.org/10.3390/min13111376

Academic Editor: Alberto De Bonis

Received: 19 September 2023
Revised: 21 October 2023
Accepted: 25 October 2023
Published: 28 October 2023

Talc is widely used in the ceramics industry for the production of various ceramic products, including steatite and cordierite ceramics. The quality requirements for talc used in ceramics vary depending on the specific application and desired properties of the final product. The production of steatite and cordierite ceramics demands high-quality talc concentrates with low impurity levels, such as iron and calcium [17–21]. For example, talc concentrate suitable for the electrical industry should not contain more than 1.5% FeO and CaO [7]. Such specifications restrict the use of talc extracted from ultramafic-derived soapstones.

In the Republic of Karelia, northwest of Russia, manufactures utilize soapstone as a construction material for fireplaces due to its capability to heat up faster than traditional red bricks and retain heat 2.5 times longer, ensuring long-lasting warmth emission. Owing to its excellent thermal stability, soapstone has been widely used as versatile raw material for the fabrication of heat-retaining cookware; hence, it is called "pot stone" [22,23]. Furthermore, it has been utilized as construction material, serving as both cladding and decorative elements in architectural designs, and for the creation of sculptural works [22].

Soapstone production generates a significant amount of fine fraction waste, which poses a challenge for soapstone processing enterprises worldwide. Despite the widespread use of soapstone, the potential applications of soapstone waste are not sufficiently studied, leading to difficulties in waste disposal. Several investigations have been conducted to evaluate soapstone waste's possible applications. Studies on the adsorption capacity of soapstone waste have identified its potential use as an adsorbent for oil spills. Soapstone powder impregnated with diesel fuel has been utilized as raw material for producing ceramics [24,25]. It has been shown that soapstone waste powder can be used as a binding material in construction [26]. Soapstone waste displays promise as a finely ground modifying additive to clay for the production of high-strength ceramic products [27].

Cladding ceramic materials are currently in demand for enhancing the aesthetic appeal of stoves and fireplaces. In the production of such materials, clay is the key component in the raw mixtures used for subsequent manufacturing [28–31]. To improve the thermal insulation properties of ceramics and to provide specific physical and mechanical characteristics to the final products, additives are incorporated into the clay mixture [32–34]. Various technogenic waste products resulting from the processing (enrichment, sawing up) of rocks are used as modifying additives for ceramics. Such waste products contain quartz, feldspar, carbonate, and ferruginous minerals, improving the properties of the products. Research studies [35,36] have shown that magnesium silicates can also be used as additives to clay in order to improve the mechanical strength of ceramics. Minerals such as talc, magnesite, and tremolite are of interest for improving the mechanical and thermal insulation characteristics of cladding ceramics. The primary objective of the present study is to develop a ceramic mixture composition for obtaining ceramics with high strength and thermal resistance by using local fusible clays as the main components of the blend and soapstone processing waste as an additive.

2. Materials and Methods

2.1. Materials

2.1.1. Geological Setting

In the present study, clays from two deposits were used to compare the composition and properties of the cladding materials. The clays are related to the Vendian–Cambrian sedimentary basins of the Baltic monocline in the central part of the East European Platform (see Figure 1) [37]. The Vendian Ivinskoe clay deposit is located 5–6 km southeast of Ladva Village, Republic of Karelia. It is associated with marine sediments, mainly clays with siltstone and sandstone interlayers, of the upper Vendian Kotlinsky suite. The deposit is not quarried at present. However, it is one of the most promising in terms of reserves prepared for industrial development. The Ivinskoe clay deposit has mainly been studied as a source of raw material for brick production [38,39], and has received little attention in terms of investigating its potential for cladding ceramics. The Cambrian "blue clays" of the Chekalovskoe deposit are related to the Lontova horizon of the Lower Cambrian

unit occurring 0.5 km northeast of Nikolskoe Town, the Leningrad Region. The productive formation consists of a clay sequence with scarce sandstone and siltstone intercalations. The Chekalovskoe clays are quarried using the open-pit method and utilized by the JSC "NEPHRITE-CERAMICS" company for the production of ceramic tiles.

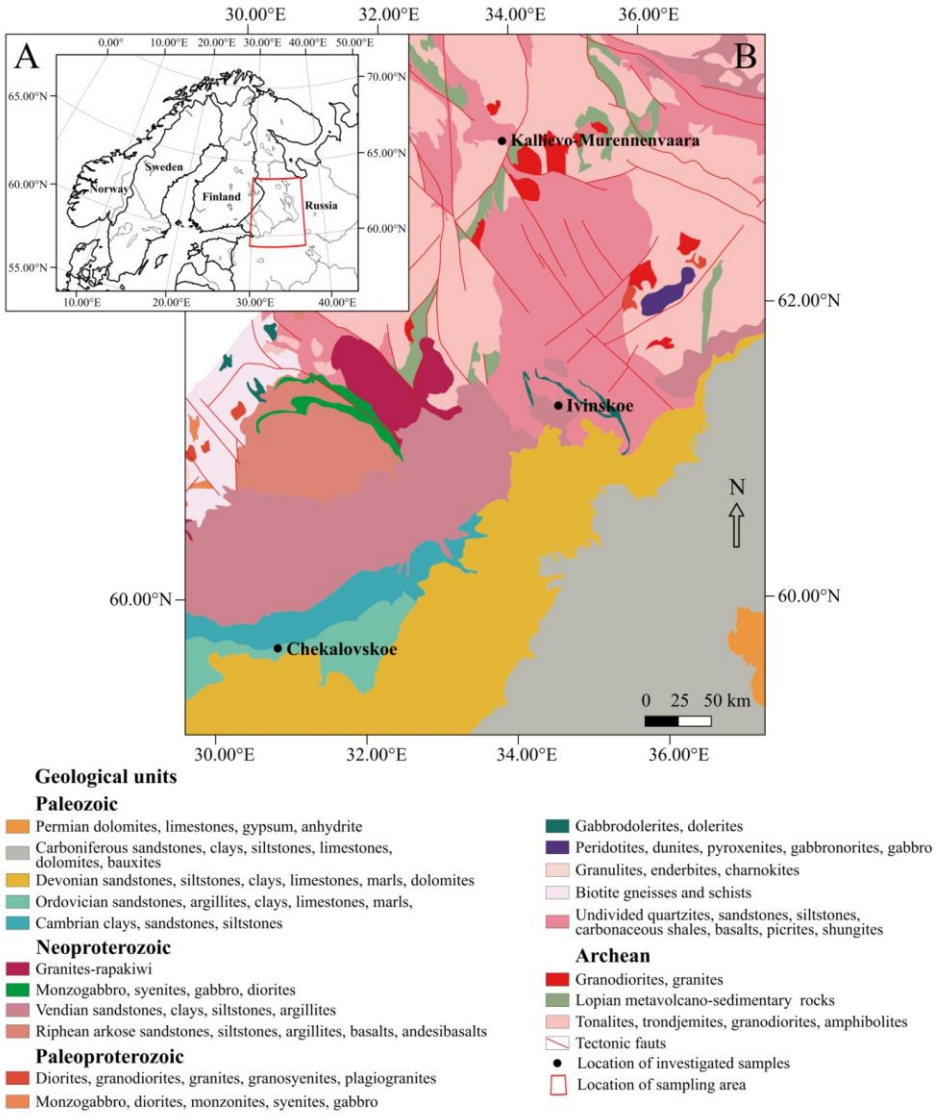

Figure 1. (**A**) Location map of the clay and soapstone deposits studied. (**B**) Simplified geological map of the central part of the East European Platform showing the location of the studied deposits (based on [40]).

The Kallievo–Murennenvaara soapstone deposit is associated with Archean ultramafic metavolcanic rocks occurring as relics of greenstone sequences within granite-gneiss country rocks in the Karelian Craton of the Fennoscandian Shield. The soapstone quarry is located 8 km west of the Velikaya Guba Village, Republic of Karelia, on the shore of Lake Segozero. Soapstone has been quarried since 1925 for manufacturing hearth tiles, electrical distribution boards, and dimension stones for building purposes.

2.1.2. Raw Materials and Sample Preparation

The Vendian clay was collected from the deposit in a quantity of 50 kg. The clay was air-dried and passed through a 1 mm sieve to eliminate thicker fragments of organic material or other impurities. The Cambrian clay, weighing 100 kg, was obtained from the JSC "NEPHRITE-CERAMICS" company and prepared for the study. Soapstone waste

powder weighing 50 kg was received from a company engaged in the manufacturing of soapstone products. In the laboratory, the powder was additionally ground in a ball mill to a fraction of less than 1 mm.

The raw materials were characterized by determining a mineralogical composition using X-ray powder diffraction (XRD) and scanning electron microscopy with energy-dispersive spectroscopy (SEM-EDS); chemical composition by X-ray fluorescence (XRF) spectroscopy; particle size distribution using laser diffraction method; thermal behavior by simultaneous differential thermal analysis and thermogravimetry (DTA-TG); and plasticity by means of Atterberg limits.

Several mixtures of the Vendian and Cambrian clays and soapstone waste were prepared by dosing and hand-mixing in a dry state with the following additions of soapstone waste: 25% (V-25 and C-25), 30% (V-30 and C-30), 35% (V-35 and C-35), and 40% (V-40 and C-40) by weight, respectively. Quartz sand (up to 5%) was partly added to the Vendian clay because its SiO_2 content was lower than in the Cambrian clay.

The preparation of samples for studying technological properties was carried out as follows. To obtain a molding mass, the mixture was moistened until it reached a moisture content of 8 wt.%. The mass was then weighed on scales to 65 g, placed in a metal mold measuring 50 mm × 50 mm × 10 mm with a metal substrate, and a metal casting rod was applied. Subsequently, the mixture was pressed on a hydraulic press at a constant pressure of 3 kN/m^2, and the resulting tile sample was removed from the mold.

The samples were dried at ambient temperature in an atmosphere for 24 h and then in a SNOL 3.5/3M muffle furnace at 95–100 °C for 2 h. Subsequently, the samples were fired at a rate of 2–3 °C/min up to temperatures of 950, 1000, 1050, and 1100 °C using a SNOL 1.6/1300 muffle furnace for 60 min of soaking time at each temperature. The samples were cooled together with the furnace.

The fired experimental samples (in a quantity of 12) were characterized in terms of technological properties: linear firing shrinkage, water absorption, density, flexural strength, thermal conductivity, specific heat capacity, and thermal shock resistance.

Measurements of thermal conductivity and specific heat capacity were conducted on 12 tablet samples with a diameter of 15 mm and a height of up to 10 mm. A diamond core drill bit was used to produce the tablet samples from the tiles.

2.2. Methods

The major element composition of the raw materials was determined by XRF spectroscopy using an ARL ADVANT'X-2331 (Thermo Fisher Scientific, Ecublens, Switzerland) wavelength-dispersive spectrometer with a rhodium tube, a working voltage of 60 kV, a working current of 50 mA, and a resolution of 0.01. Preliminarily, 2 g of each powdered sample were heated in ceramic crucibles at 1000 °C in a muffle furnace for 30 min. The loss on ignition (LOI) was determined by a change in the mass of the sample after heating. For XRF measurements, 1 g of heated sample was mixed with Li-tetraborate flux and heated in an Au-Pt crucible to 1100 °C to form a fused bead.

The XRD patterns of the powder samples were recorded on a Thermo Scientific ARL X'TRA (Thermo Fisher Scientific, Ecublens, Switzerland) diffractometer using Bragg–Brentano geometry and CuKα radiation (γ = 0.1790210 nm). Operating conditions were as follows: 40 kV accelerating voltage, 30 mA current, scanning range 5–75° 2θ, and scanning step of 0.40 2θ/min. The XRD investigations of clays were carried out on bulk samples and clay fractions using randomly oriented powder mounts and oriented aggregate mounts, according to the methodology presented by [41]. The <2 μm fractions were collected by Stokes settling. The oriented aggregate mounts were prepared by allowing clay–water suspensions to dry at room temperature on a glass slide. The XRD patterns of the clay fraction were recorded under natural conditions, after saturation with glycerol for 22–24 h, and after heating at 550–600 °C for 1.5 h. The mineral phases were identified using WinXRD software Version 2.0-6 and the ICDD database. A semi-quantitative determination of the relative abundances of phases was performed by the Rietveld method using SIROQUANT software

Version 3.0. The weight percent of the X-ray amorphous component was determined by the external standard method, with ZnO used as the standard. The detection limit was 3 wt%.

SEM-EDS investigations were conducted on carbon-coated samples using a VEGA II LSH (Tescan, Brno, Czech Republic) scanning electron microscope with an SDD X-Act3 energy-dispersive detector (Oxford Instruments, Oxford, UK). Operating conditions were as follows: W cathode, 20 kV accelerating voltage, 20 nA beam current, 2 µm beam diameter, 90 s counting time. SEM-EDS quantitative data were acquired and processed using the Microanalysis Suite Issue 12, INCA Suite version 4.01. Natural mineral standards were used to calibrate the raw data.

DTA-TG analyses were carried out using NETZSCH STA 449 F1 Jupiter equipment (Selb, Germany) over the temperature range of 20–1000 °C in an air atmosphere at a heating rate of 10 °C/min. The powdered samples were placed into a platinum–rhodium crucible in the amount of 10 mg.

Granulometric analysis was performed by laser diffraction method using an LS 13 320 Beckman Coulter particle size analyzer.

All analysis were carried out at the Centre for Collective Usage, Karelian Research Centre, RAS (Petrozavodsk, Russia).

The liquid limit, plastic limit, and plasticity index were determined according to [42] using the cone penetrometer method as the liquid limit test and the roll-forming method as the plastic limit test. The difference between both values reflected the plasticity index.

Linear firing shrinkage was calculated based on standard [43] according to Equation (1):

$$Y = \frac{ld - lf}{ld} \times 100 \quad (1)$$

where *ld* and *lf* are measured lengths of dried and fired sample, respectively.

Flexural strength was estimated using the three-point bending method according to [44]. The average flexural strength values were calculated using Equation (2):

$$\sigma = \frac{3FL}{2bh^2} \quad (2)$$

where *F* is the breaking load, kg; *L* is the distance between supports (*L* = 29.67 mm); *b* is the width of the sample, mm; and *h* is the thickness of the sample, mm.

Density was defined using the hydrostatic weighing method according to [45]. The apparent density was calculated using Equation (3)

$$P = \frac{mi - pl}{mf - mb} \quad (3)$$

where *mi* is the mass of the dry sample weighed in air, g; *pl* is the density of water; *mf* is the mass of the sample saturated with water, g; and *mb* is the mass of weights balancing the mass of the sample immersed in water, g.

Water absorption was determined according to [45]. The water absorption (W) value was calculated using Equation (4):

$$W = \frac{Wf - Wi}{Wi} \times 100\% \quad (4)$$

where *Wi* and *Wf* are the sample weights before and after immersion, respectively.

The thermal conductivity coefficient was determined on an ITEM-1M meter using the steady-state method. Specific heat capacity was measured on an IT-S-400 meter using a dynamic method of heating [46].

Thermal shock resistance was determined by measuring the amount of thermal shock cycles samples could withstand when heated to 950 °C and 1100 °C, held at that temperature for 30 min, and then cooled for 5 min in flowing water, without being destroyed.

3. Results and Discussion

3.1. Granulometric Study and Atterberg Limits

The laser diffraction particle size analysis of the clays studied indicates the predominance of silt and clay fractions. The clays refer to medium-dispersed raw materials with a low content of coarse-grained inclusions (>2 mm). The clay fraction content is about 13% for both clays (see Table 1). The summary content of clay and silt fractions is 70.22% and 76.52% for the Vendian and Cambrian clays, respectively.

Table 1. Particle size distribution of the investigated raw materials used in clay/soapstone mixtures.

		Vendian Clay	Cambrian Clay	Soapstone Waste
Particle fractions	<2 μm	12.28	13.63	6.37
	2–20 μm	57.94	62.89	50.62
	>20 μm	29.78	23.48	43.00
	Mean particle size, μm	7.55	9.12	16.87
Particle size distribution	Diameter for 10% (D10), μm	1.40	1.56	3.41
	Diameter for 50% (D50), μm	7.55	10.67	18.52
	Diameter for 90% (D90), μm	39.67	37.62	81.22

The cumulative particle size distribution (see Figure 2, Table 1) demonstrates that the particle size range is similar in both clays (D10–D90: 1.40–39.67 μm and 1.56–37.62 μm), with median (D50) values of 7.55 μm and 10.67 μm for the Vendian and Cambrian clays, respectively. The Vendian clay has an average particle size value that coincides with the median particle diameter (D50) of 7.55 μm, indicating a uniform particle size distribution.

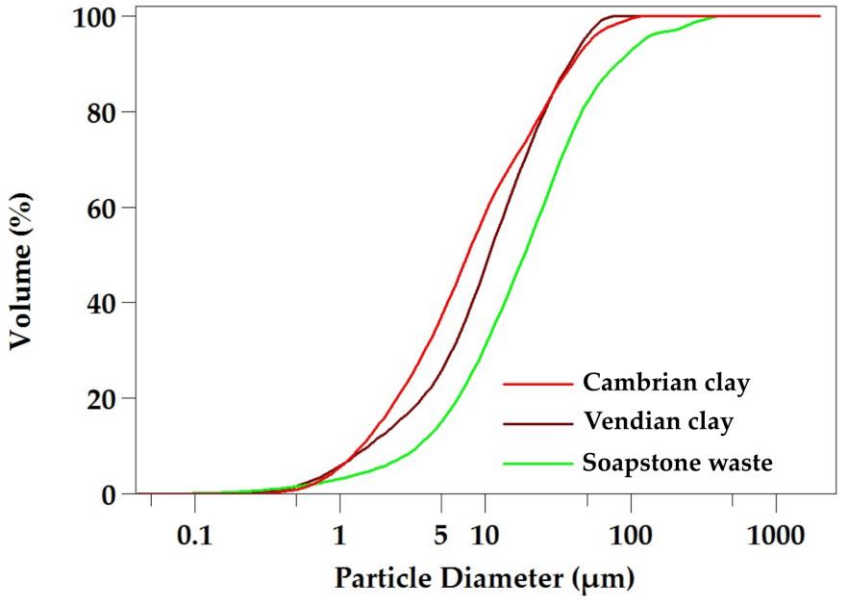

Figure 2. Cumulative particle size distribution of the raw materials.

Soapstone waste is characterized by a lower concentration of clay and silt fractions compared to the clays, with 6.37% and 50.62%, respectively. The cumulative curve shows a coarser grain size of soapstone waste with a higher median particle diameter (D50) of 18.52, which is significantly larger than that of the clays. Considering the D10 and D90 values, it can be observed that soapstone waste has a larger particle size range, indicating its polydispersity (D10–D90: 3.41–81.22 μm).

In order to evaluate the behavior of the clays in terms of plastic limit and liquid limit, an Atterberg limits test was carried out. The liquid limit of clay samples varies from 32.8% to 38% for the Vendian clay and from 42.2% to 48% for the Cambrian clay. The

liquid limit values of the investigated clays are within the range defined for compositions applicable for ceramic manufacturing (30%–60%) [47]. The Vendian clay shows the plastic limit ranging between 16.9% and 17.4%, while the plastic limit values of the Cambrian clay vary from 17.6% to 24.8%. The plasticity index values of the clay samples are in the range of 15.4%–21% and 19.6%–30% for the Vendian and Cambrian clays, respectively. Presumably, such values are attributed to the predominance of the silt fraction in the studied clays. The plasticity parameters indicate that the studied clays belong to the inorganic medium plastic clays (according to the Casagrande classification [48].

The addition of soapstone waste to clay reduces the plasticity of the mixture. The plasticity index values of the mixture containing 40% soapstone waste range from 12.15% to 16.62% for the Vendian-clay-based mixtures and from 15.73% to 23.65% for the Cambrian-clay-based ones.

3.2. Mineralogical Study

The XRD patterns of the bulk samples, as well as the oriented clay fractions of the clays, are presented in Figure 3.

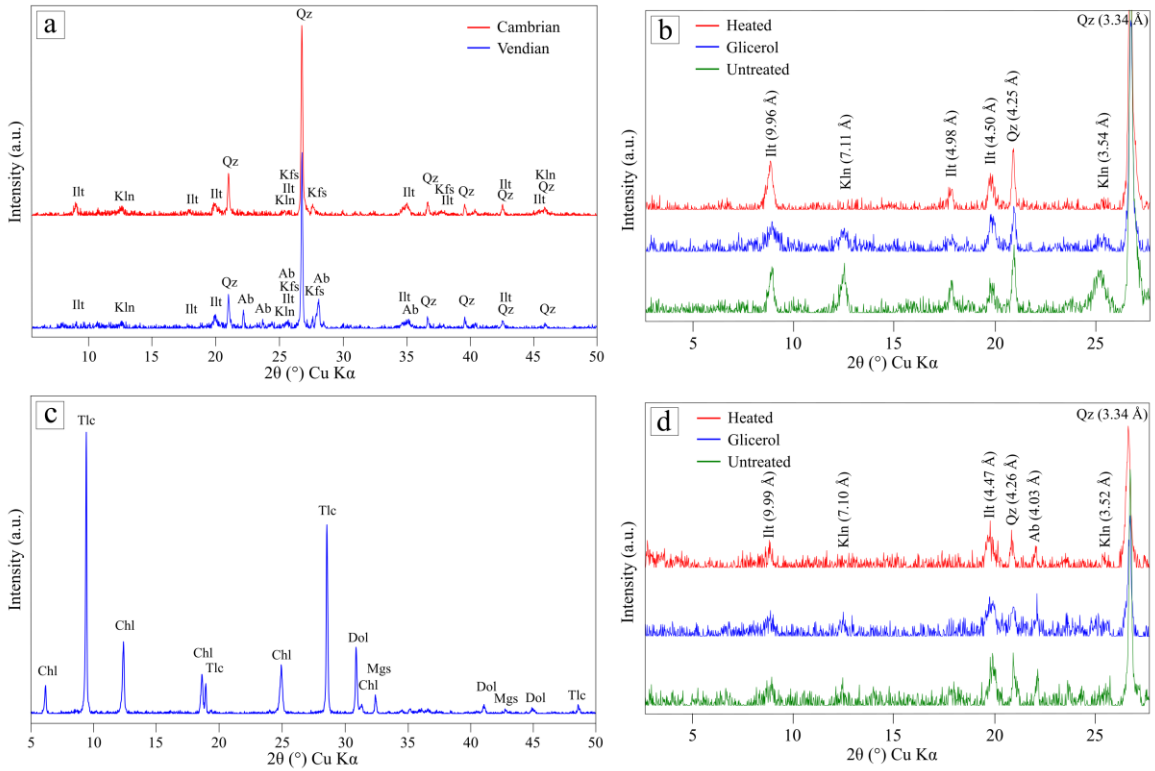

Figure 3. XRD patterns of the bulk samples of the clays (**a**) and soapstone waste (**c**), and XRD-oriented patterns of the clay fraction of Cambrian (**b**) and Vendian (**d**) clay under natural conditions (untreated sample), saturated with glycerol, and heated at 550–600 °C. Ab—albite, Mgs—ferroan magnesite, Chl—chlorite, Dol—dolomite, Ilt—illite/glauconite, Kfs—K-feldspar, Kln—kaolinite, Tlc—talc, Qz—quartz.

The XRD analysis results of the whole rock samples indicate that the clays studied comprise variable amounts of quartz (the basal reflection d (101) at 3.34 Å), feldspars (K-feldspar (d (040) at 3.24 Å) and albite (d (002) at 3.19 Å)), and clay minerals such as illite/glauconite (d (001) at ~10 Å) and kaolinite (d (001) at 7.13 Å). According to semi-quantitative analysis using the Rietveld method, the clays are characterized by the dominance of phyllosilicates. The content of illite/glauconite is 42% and 47% in the Vendian and Cambrian clays, respectively. The percentage of kaolinite is relatively low, at 4% in the Cambrian clay and 7% in the Vendian clay. Non-clay minerals in the Cambrian clay

are represented by the predominant quartz (43%) and a small amount of K-feldspar (6%), while, in the Vendian clay, they are present in equal amounts of quartz (22%) and albite (21%) with a low content of K-feldspar (8%).

The XRD patterns of the clay fractions of the clays (see Figure 3b,d) show reflections at 7.10–7.11 Å and 3.52–3.54 Å, which disappear after heating at 550–600 °C, confirming the presence of the kaolinite phase. The clay fraction of the Cambrian clay is rich in illite/glauconite (84%) and also contains quartz (6%) as well as kaolinite (10%). The Vendian clay's clay fraction comprises a lesser amount of illite/glauconite (74%), albite (12%), kaolinite (5%), and trace amounts of K-feldspar.

Figure 4 shows the SEM images of the investigated samples. The results of SEM-EDS study are in agreement with the XRD data. According to the EDS analysis, the predominant clay minerals are represented by both illite and glauconite. Compared to illite, glauconite exhibits elevated concentrations of Fe, Mg, K, Ti, and a lower abundance of Al, as observed in the EDS patterns (see Figure 4h). Kaolinite is present in minor amounts compared to the hydromica content. In the sand and silt fractions, the proportion of clay mineral aggregates is reduced, and dispersed non-clay minerals such as quartz and feldspars (albite in the Vendian clay and K-feldspar in the Cambrian clay) prevail. Additionally, trace amounts of dolomite, pyrite, and Fe oxides were revealed.

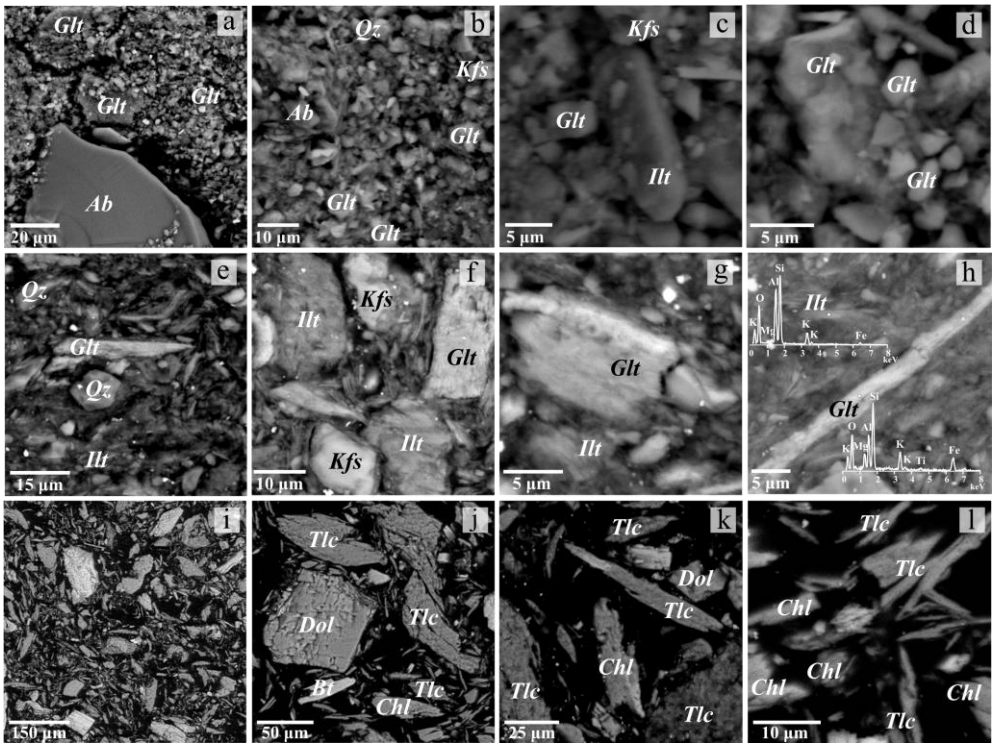

Figure 4. SEM-BSE images of ground Vendian (**a**–**d**) and Cambrian (**e**–**h**) clay, and soapstone processing waste (**i**–**l**). The insets in (**h**) show the EDS patterns of illite and glauconite. Ab—albite, Bt—biotite, Chl—chlorite, Dol—dolomite, Glt—glauconite, Ilt—illite, Kfs—K-feldspar, Tlc—talc, Qz—quartz.

The concentration of clay minerals such as illite and kaolinite in the clay fraction is the main factor determining the technological properties of clay raw materials and the quality of ceramics produced from them [49–52]. Based on the mineralogical composition, it is evident that the abundance of clay minerals results in medium plasticity of the studied clays. It is assumed that feldspars will act as a flux in the ceramic mass, forming a liquid phase at high temperature that allows to densify the ceramic body by a viscous flow [28,53].

The powder diffraction pattern of soapstone processing waste (see Figure 3c) shows the presence of talc (35%) (the basal reflection d (002) at 9.36Å), chlorite (28%) (d (001) at 14.25Å, d (002) at 7.13Å), dolomite (26%) (d (104) at 2.89Å), and ferroan magnesite (11%)

(d (104) at 2.76Å) as major phases. Ore minerals such as magnetite, chromite, and sulfides were identified by the SEM-EDS study. According to the EDS analysis results, in addition to dolomite and ferroan magnesite (iron content of 15–18 wt.% FeO), soapstone contains calcite with isomorphic impurities of magnesium (17 to 20 wt.% MgO) and iron (3 to 9 wt.% FeO). Talc is characterized by an elevated iron content of 4–5 wt.% FeO, which is a common feature of talc associated with ultramafics. Carbonate minerals form isometric grains, while silicates mainly occur as elongated plates (see Figure 4k,l). In coarser fractions, minerals occur in polymineral intergrowths (see Figure 4k). Fine classes (1–60 µm), constituting a significant portion of the material (>88%), commonly contain no intergrowths (see Figure 4l). It is expected that the presence of talc will increase the heat resistance and strength of the ceramics, while MgO and CaO oxides formed from carbonates during firing will act as fluxes, facilitating the formation of low-melting eutectics, particularly with silica [32]. The carbonates will serve as a pore-forming agent, which develops porosity during firing and facilitates sintering through surface diffusion [28].

3.3. Chemical Study

For efficient application, the chemical compositions of clays and soapstone waste were analyzed.

The clays studied are characterized by a similar major element distribution, consisting mainly of SiO_2, Al_2O_3, Fe_2O_3, K_2O, MgO, and Na_2O, while TiO_2, MnO, and P_2O_5 occur in relatively low concentrations (see Table 2). The chemical composition of the clays is consistent with their mineralogy. The high SiO_2 contents are associated with increased amounts of quartz. The concentrations of Al_2O_3 are primarily influenced by the abundance of clay minerals, and to a lesser extent by the presence of K-feldspar. The Vendian and Cambrian clays contain a high amount of alkali oxides (K_2O + Na_2O)—5.48% and 5.32%, respectively. The most significant difference between the clays is the low content of Na_2O in the Cambrian clay. The increased concentration of Na_2O in the Vendian clay is associated with the presence of a significant amount of albite in the rock. The high content of K_2O indicates the presence of hydromica minerals, as well as K-feldspar. According to reference [54], hydromica clays typically have a K_2O content ranging from 4 to 6.23%. The primary impact of alkalis on clays is the reduction of their refractory properties. The elevated Fe_2O_3 content of the clays might be attributed to the glauconite abundance. A high Fe_2O_3 content of clays produces red-colored ceramics [28]. However, red tiles could be acceptable for furnace insulation. The high amount of alkalis and Fe_2O_3, as well as low concentration of Al_2O_3 compared to kaolin (up to 45%), indicate low fusibility of the clays. In terms of Al_2O_3 content in the calcined state, the clays analyzed refer to semi-acidic clay materials.

Due to the mineralogy, dominated by talc, ferroan magnesite, dolomite, and chlorite, the soapstone waste is characterized by high concentrations of SiO_2, MgO, Fe_2O_3, Al_2O_3, and CaO. It contains no alkaline oxides. The increased amount of LOI is attributed to the significant carbonate content present.

The ceramic mixtures of a specific formulation based on the Vendian and Cambrian clays are characterized by a similar distribution of major elements, differing mainly in the concentration of Na_2O and K_2O (see Table 2). The most significant differences in the chemical composition of mixtures depending on the content of soapstone waste additives are observed for oxides such as SiO_2, Al_2O_3, and MgO, as well as for LOI. Increasing the amount of additives into each clay leads to a gradual simultaneous decrease in the content of SiO_2 and Al_2O_3, and an increase in the concentrations of MgO and LOI. The high amount of alkaline oxides in the mixtures, reacting with silica and alumina, will facilitate the formation of a liquid phase that promotes densification and sintering at relatively low temperatures.

Table 2. Chemical composition of raw materials, as well as the formulation and calculated chemical composition of the clay/soapstone waste mixtures (wt.%).

	Wt.%	V	C	S	V-25	V-30	V-35	V-40	C-25	C-30	C-35	C-40
Chemical composition	SiO_2	60.44	62.97	33.35	55.64	54.28	52.93	51.58	55.57	54.09	52.61	51.13
	TiO_2	0.85	0.90	0.16	0.64	0.60	0.57	0.53	0.72	0.68	0.64	0.60
	Al_2O_3	16.64	16.79	4.14	12.68	12.06	11.43	10.81	13.63	13.00	12.36	11.73
	Fe_2O_3 *	5.41	4.73	10.73	6.48	6.74	7.01	7.28	6.23	6.53	6.83	7.13
	MnO	0.09	0.04	0.17	0.11	0.11	0.11	0.12	0.07	0.08	0.09	0.09
	MgO	2.44	2.56	27.45	8.57	9.83	11.08	12.33	8.79	10.03	11.28	12.52
	CaO	1.23	0.81	4.69	2.04	2.21	2.38	2.55	1.78	1.97	2.17	2.36
	Na_2O	1.82	0.13	-	1.27	1.18	1.09	1.00	0.10	0.09	0.08	0.08
	K_2O	3.66	5.19	0.02	2.57	2.39	2.20	2.02	3.90	3.64	3.38	3.12
	P_2O_5	0.23	0.12	-	0.16	0.15	0.14	0.13	0.09	0.08	0.08	0.07
	SO_3	0.05	0.04	0.05	0.05	0.05	0.05	0.05	0.04	0.04	0.04	0.04
	H_2O	2.18	1.09	0.02	1.53	1.42	1.32	1.21	0.82	0.77	0.72	0.66
	LOI	4.96	4.63	19.18	8.26	8.98	9.69	10.40	8.27	9.00	9.73	10.45
Formulation	Vendian clay	100			70	65	60	55				
	Cambrian clay		100						75	70	65	60
	Soapstone waste			100	25	30	35	40	25	30	35	40
	Quartz				5	5	5	5				

Note: V, C, and S represent the chemical composition of the Vendian, Cambrian clay, and soapstone waste, respectively. * Total iron as Fe_2O_3. A hyphen indicates below detection limit.

3.4. Thermal Analysis

The thermal behavior of the raw materials was determined by the results of differential thermal and associated thermogravimetric analysis, presented in Figure 5.

The thermogravimetric curves of the investigated clays show several steps of mass loss accompanied by both endothermic and exothermic peaks. For both clays, the first significant endothermal effect occurring from room temperature to 180 °C, associated with the mass loss of 2%–3%, is connected to adsorbed and interlayer water removal ascribed to layered silicates. The presence of an exothermic effect with a peak maximum at about 320 °C, accompanied by the mass loss of 0.6%–2%, is attributed to the organic matter combustion. The broad endothermic peak within the temperature range of 400 to 780 °C, which coincides with a significant mass loss (about 3%) on the TG curves, suggests a superposition of more than one endothermic effect related to the dehydroxylation of hydromicas and kaolinite accompanied by phase transitions into dehydroxylated phases [55–59]. The destruction of the illite lattice appears within the temperature range of 870–890, expressing as a weak endothermic effect. In addition, the small exothermic peak at ~920 °C is regarded as corresponding to the formation of a spinel phase [57,60–62].

The differentiated thermal analysis of soapstone waste demonstrates that the decomposition of chlorite is characterized by a two-step dehydroxylation behavior accompanied by two endothermic effects [63]. The first step is related to the dehydroxylation within the brucite layer in the temperature range between 510 °C and 650 °C. The second step is due to the removal of the remaining OH groups from the talc-like 2:1 layer at a higher temperature interval from 750 °C to 840 °C. The exothermic effect occurring at nearly 840 °C, immediately after the second chlorite dehydroxylation peak, is attributed to the formation of new phases (olivine, spinel) representing the chlorite recrystallization products [61]. The endothermic decomposition reaction of ferroan magnesite, accompanied by the carbon dioxide releasing and magnesium oxide formation, occurs within the temperature range of the first endothermic effect of chlorite dehydroxylation, contributing to the mass loss. The endothermic effect with a peak maximum at about 730 °C is attributed to the decomposition of dolomite. The corresponding mass loss of 7% is associated with the releasing of carbon dioxide and accompanying formation of calcite and magnesium oxide [61]. It is assumed that subsequent decomposition of calcite occurs in the temperature range related to the dehydroxylation and structure decomposition of talc. This endothermic effect has a peak

maximum of nearly 950 °C. The decomposition of talc is associated with the formation of enstatite and amorphous silica [64].

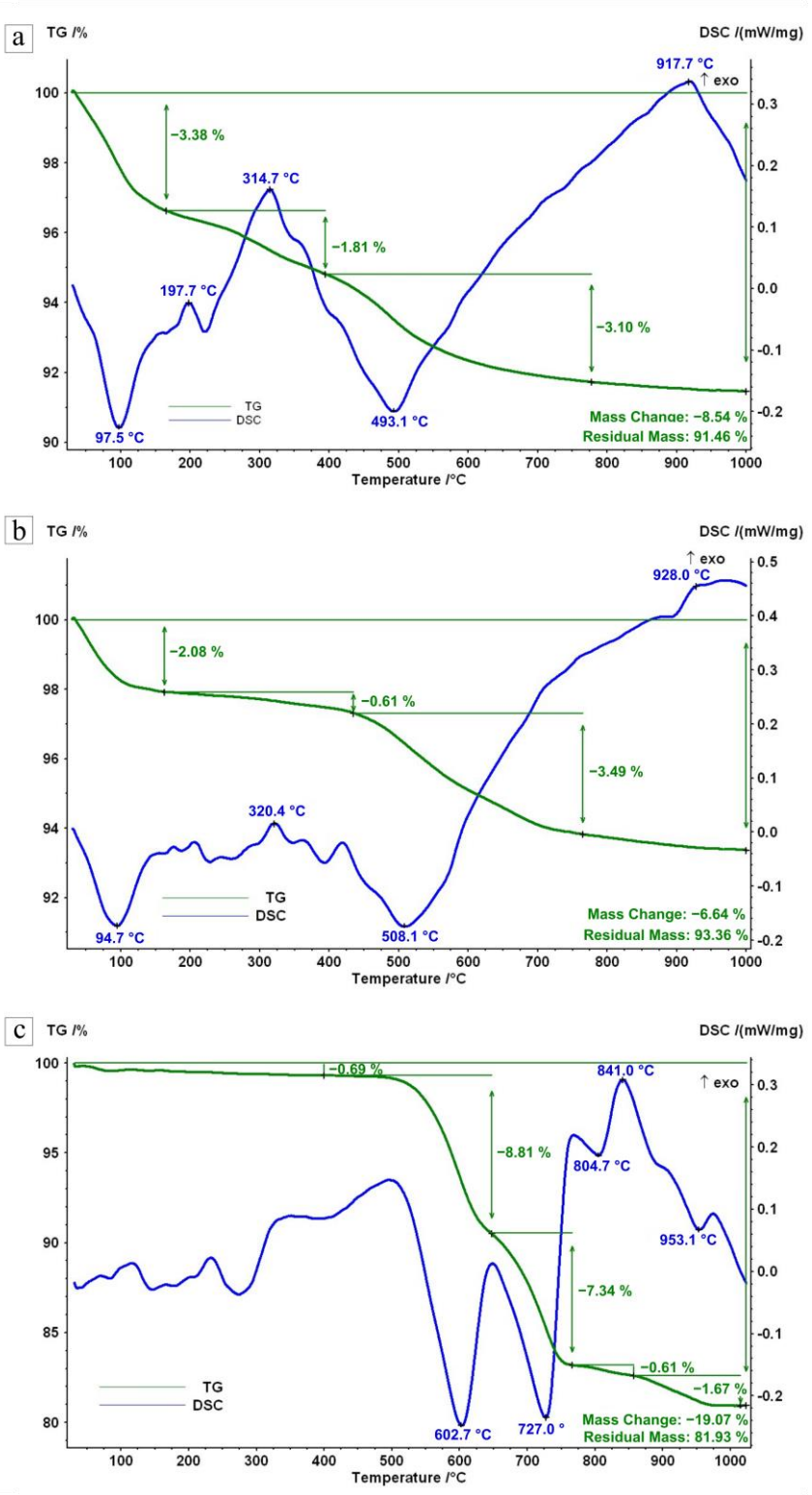

Figure 5. DTA-TG curves of the Vendian (**a**) and Cambrian (**b**) clays and soapstone waste (**c**).

3.5. Ceramic Properties

The properties of ceramics with finely ground soapstone waste additives were investigated according to the quality requirements of ceramic materials. The fired ceramic samples were tested to determine linear firing shrinkage, density, water absorption, and

flexural strength. The dependence of ceramic properties on the percentage of soapstone waste additives in samples fired at 1100 °C and the heat-treating temperature of samples containing 40% soapstone waste is presented in Tables 3 and 4, respectively.

Table 3. Technological properties of ceramic tiles fired at 1100 °C.

Property	Unit	V-25	V-30	V-35	V-40	C-25	C-30	C-35	C-40
Density	g/cm^3	1.91 ± 0.07	1.96 ± 0.05	1.99 ± 0.06	2.02 ± 0.05	1.96 ± 0.07	1.98 ± 0.06	1.99 ± 0.08	2.12 ± 0.14
Linear firing shrinkage	%	10.32 ± 1.9	9.43 ± 2.8	9.12 ± 1.6	8.32 ± 0.06	11.19 ± 0.5	10.82 ± 2.0	9.76 ± 0.5	8.57 ± 0.3
Water absorption	wt.%	16.56 ± 0.7	16.58 ± 1.1	16.60 ± 0.15	16.65 ± 0.05	16.74 ± 0.4	16.76 ± 0.02	16.78 ± 0.08	16.81 ± 0.04
Flexural strength	MPa	25.53 ± 0.08	29.33 ± 0.09	33.64 ± 0.1	37.54 ± 0.1	25.18 ± 0.06	29.87 ± 0.1	32.54 ± 0.12	35.05 ± 0.1

Table 4. Technological properties of ceramic tiles containing 40% soapstone waste fired at maximum temperatures of 950, 1000, 1050, and 1100 °C.

Property	Unit	V-40				C-40			
		950	1000	1050	1100	950	1000	1050	1100
Density	g/cm^3	1.91 ± 0.07	1.98 ± 0.06	1.99 ± 0.06	2.02 ± 0.05	1.91 ± 0.07	1.95 ± 0.07	1.98 ± 0.07	2.12 ± 0.14
Linear firing shrinkage	%	7.02 ± 0.9	7.90 ± 0.07	8.12 ± 0.06	8.32 ± 0.06	7.43 ± 0.06	8.15 ± 0.06	8.51 ± 0.04	8.57 ± 0.3
Water absorption	wt.%	17.15 ± 0.04	16.81 ± 0.05	16.73 ± 0.06	16.65 ± 0.05	17.56 ± 0.07	17.53 ± 0.08	17.42 ± 0.07	16.81 ± 0.04
Flexural strength	MPa	21.42 ± 0.06	24.30 ± 0.7	34.67 ± 0.05	37.54 ± 0.1	20.05 ± 0.09	26.68 ± 0.07	28.31 ± 0.04	35.05 ± 0.1

As can be seen in Table 3, the density, firing linear shrinkage, and water absorption values of the samples based on the Cambrian and Vendian clays are similar and vary slightly depending on the ratio of clay to soapstone waste additive in the ceramic mixture. When increasing the addition of soapstone waste from 25% to 40%, the density values of ceramic samples with the Vendian clay increase by 1%–3%, while those with the Cambrian clay rise by 2%–3%. According to [65,66], the presence of magnesium silicates in the original mixture tends to promote the development of a less viscous liquid phase, providing higher reactivity and improving densification. The slight water absorption rise is presumably related to an increase in porosity resulting from the decomposition of carbonates and silicates, comprising soapstone, during the heat treatment, as more soapstone waste is added. The gradual increase in the addition of soapstone waste leads to a decrease in linear firing shrinkage associated with an increase in porosity. The linear firing shrinkage values of the samples based on the Cambrian clay are higher than those in the formulations with the Vendian clay due to the elevated content of fine-size clay mineral particles in the mixtures.

The results indicate that the addition of 25% to 40% of soapstone waste to clay in ceramic mass fired at 1100 °C has a positive effect on the flexural strength of the samples. The flexural strength is significantly increased in samples containing both the Vendian and Cambrian clays with the addition of 40% soapstone waste. Moreover, the flexural strength values of the Cambrian-clay-based samples are only 2%–3% lower compared to specimens containing the Vendian clay with the addition of 5% finely dispersed quartz sand. The high values of flexural strength (over 37 MPa) of the experimental samples fired at 1100 °C meet the requirements of the European standard [67] for dry-pressing ceramic tiles, classifying into Group B III (with a water absorption greater than 10%).

In order to investigate the effect of firing temperature on the overall shrinkage, water absorption, and flexural strength of ceramics, an interval ranging from 950 °C to 1100 °C was chosen. Under these temperature conditions, construction ceramic materials such as bricks (fired at 950 °C) and ceramic tiles (fired at 1100 °C) undergo heat treatment during the manufacturing process at JSC "NEPHRITE-CERAMICS". The mixture containing 40% soapstone waste additive was selected as representative as it demonstrated the best flexural strength values for both the Vendian and Cambrian clays.

The firing temperature significantly affects the water absorption and linear firing shrinkage of ceramic samples. As can be seen in Table 4, an increase in the temperature of

heat treatment is accompanied with the progressive increase in the linear firing shrinkage and a decrease in the water absorption values. This is presumably related to the progressive increase in the amount of a liquid phase, responsible for the densification of the final product, as the temperature rises. The values of these parameters are similar for samples based on both clays and differ within a range of 2%–3%. Sharp changes in the values of these parameters, observed above 1050 °C, indicate active sintering [68].

The flexural strength values of the ceramic samples increase as the firing temperature rises within the temperature range of 950–1100 °C. A noticeable enhancement initiates at a firing temperature of 1000 °C and increases significantly at 1050 °C. It is assumed that the formation of a liquid phase, which produces the glass or vitreous phase after cooling the ceramics, along with the formation and growth of new crystalline phases due to the processes of decomposition and recrystallization of minerals constituting the raw materials facilitated the strength increase of the test samples.

The results of XRD analysis of a ceramic sample containing 40% soapstone waste, 55% Vendian clay, and 5% finely dispersed quartz sand fired at 1100° (see Figure 6) revealed that the ceramic composition essentially comprises enstatite (32 ± 1.9 wt.%), quartz (15 ± 0.6 wt.%), albite (19 ± 1.3 wt.%), diopside (12 ± 1.3 wt.%), hematite (9 ± 0.6 wt.%), and a glassy (amorphous) phase (13 ± 3.6 wt.%). The abundant quartz and albite are the original minerals that persisted during firing. It is assumed that enstatite was formed due to the decomposition predominantly of talc and, to a lesser extent, chlorite [55,64]. The spinel and olivine phases may not have been observed, possibly due to the overlapping of their XRD peaks with peaks of other phases, or, alternatively, the abundance of CaO prevented their crystallization from the decomposition of clay minerals. Presumably, the dehydroxylation of illite, glauconite, kaolinite, and chlorite and reacting with CaO derived from the dissociation of dolomite facilitated the formation of a Ca-rich aluminosilicate phase such as diopside [69–72]. The presence of hematite could be related to the iron released during the decomposition of ferruginous glauconite, illite, magnesite, and chlorite.

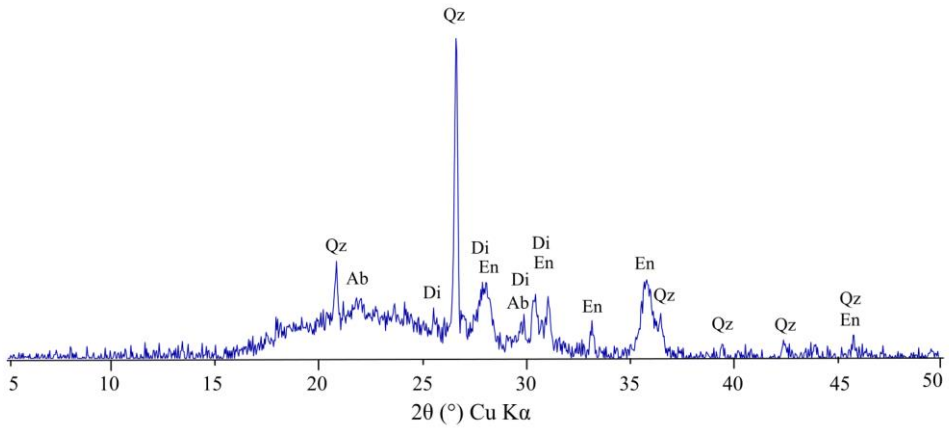

Figure 6. XRD pattern of a ceramic sample containing 40% soapstone waste, 55% Vendian clay, and 5% finely dispersed quartz sand fired at 1100 °C. Ab—albite, Di—diopside-augite, En—enstatite, Qz—quartz.

The results demonstrate that the formation of pyroxenes contributes significantly to the improvement in flexural strength of the ceramic samples with soapstone additives.

Considering the color of the experimental ceramic samples (see Figure 7), it can be observed that they exhibit a red hue that intensifies as the temperature rises. This color variation is attributed to the significant amount of iron oxides present in the raw materials and correlates with the abundance of hematite in the fired samples [28].

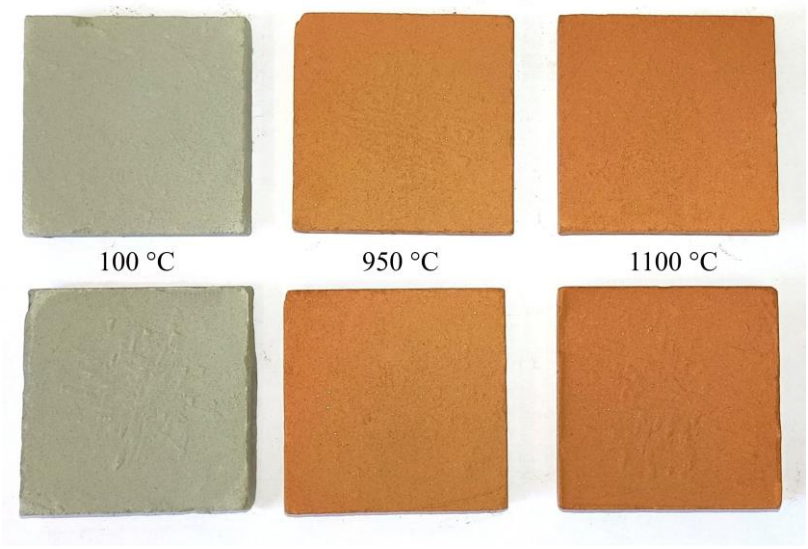

Figure 7. Experimental ceramic samples manufactured from the Vendian (**upper**) and Cambrian clay (**lower**), dried at 100 °C, and fired at 950 °C and 1100 °C.

Phase transformations, along with the formation of an amorphous phase modifying the structure of ceramics during firing, have a significant impact on both the strength and thermal properties of ceramics. The thermal properties of ceramic samples, natural soapstone, and the prototype [73] are reported in Table 5. The formation of porosity during the heat treatment of ceramic samples due to the gases released from the dehydration, dehydroxylation, and decarbonation of minerals in the raw materials has resulted in the low values of the thermal conductivity of ceramics. Increasing the heat treatment temperature from 950 to 1100 °C of the experimental samples leads to a slight decrease in the thermal conductivity and an increase in the thermal shock resistance of ceramics. Increasing the thermal shock resistance with the introduction of soapstone waste can be attributed to the relatively high porosity of ceramics, which relaxes the thermal shock stress and arrests the propagation of microcracks. The glass phase also contributes to enhancing the thermal resistance of ceramics.

Table 5. Thermal properties of the test samples.

Sample	Properties of the Samples Fired at the Temperature						
	950 °C				1100 °C		
	Specific Heat Capacity, J/kg·K	Thermal Conductivity, W/m·K	Thermal Shock Resistance, Number of Thermal Shock Cycles	Flexural Strength	Specific Heat Capacity, J/kg·K	Thermal Conductivity, W/m·K	Thermal Shock Resistance, Number of Thermal Shock Cycles
C-1	870	0.05–1.3	9–13	19	880	0.05–0.8	>18
C-2	885	0.07–1.3	7–11	22	895	0.06–0.7	>12
C-3	870	-	2–3	13–15	890	1–3	≥2
Soapstone [1]	890	0.9–1.08	7–13	-	896	2.3–2.8	7–9

C-1—Ceramic samples containing 55% Vendian clay, 40% soapstone waste, 5% quartz sand; C-2—Ceramic samples containing 60% Cambrian clay and 40% soapstone waste; C-3—Ceramic samples based on fusible clay and talc quarry waste [73]. [1] Natural soapstone from the Kallievo–Murennenvaara deposit.

Compared to the prototype (Table 5, C-3), the thermal stability and mechanical strength of the experimental samples are significantly increased. The flexural strength values of the experimental ceramic samples fired at 950 °C are 20–21 MPa, while the prototype is characterized by lower values of 13–15 MPa. The thermal shock resistance of the test samples (>7 thermal shock cycles) is significantly higher than that of the prototype (2–3 thermal shock cycles). No significant differences in the values of specific heat capacity are observed

between soapstone (Table 5) and ceramics, as well as in their variations with respect to the heating temperature.

4. Conclusions

1. The results obtained from the study have demonstrated the potential utilization of local Cambrian and Vendian clays by the addition of soapstone processing waste to produce high-strength ceramics with a flexural strength of 37.54 MPa and high thermal resistance. The ceramic samples withstand more than 18 thermal shock cycles without surface damage and exhibit a low thermal conductivity of 0.05–0.8 W/m·K.
2. An assessment of the physical and mechanical properties of products fired at 1100 °C has shown that the optimal ratio of clay and soapstone waste in the ceramic mixture is 60/40%.
3. The increase in mechanical strength and thermal stability of the produced ceramics is closely related to the formation and enrichment of a glassy phase, enstatite, and diopside as a result of processes such as decomposition, recrystallization, and interaction of minerals comprising raw materials during firing.

In conclusion, it should be noted that the recycling of soapstone processing waste in clay ceramic products (tiles, bricks) is possible with the introduction of additives of approximately 30%–40% by weight. This statement is based solely on the technological characteristics of local Vendian and Cambrian hydromica clays.

The production of ceramic products with the addition of soapstone processing waste could solve the problem of waste disposal and expand the product range of enterprises engaged in the manufacturing of fireplaces and stoves.

Author Contributions: Conceptualization, V.I. and E.K.; methodology, V.I.; software, E.K.; validation, V.I., E.K. and T.B.; formal analysis, V.I.; investigation, V.I., T.B. and E.K.; resources, V.I.; data curation, V.I., E.K. and T.B.; writing—original draft preparation, V.I.; writing—review and editing, E.K.; visualization, E.K.; supervision, V.I.; project administration, E.K. All authors have read and agreed to the published version of the manuscript.

Funding: This research was funded by state assignment to the IG KarRC RAS, according to the Research Program of the IG KarRC RAS, Reg. number 1022040400124-6-1.5.5; FMEN-2023-0005.

Data Availability Statement: The raw data supporting this study are available from the corresponding author, V.I., upon reasonable request.

Acknowledgments: The authors would like to acknowledge Irina S. Inina for her assistance with the XRD investigation and express gratitude to the three anonymous reviewers for their valuable comments, which have helped to improve the manuscript. Alexandra Skvortsova is sincerely appreciated for her assistance in preparing the geological map.

Conflicts of Interest: The authors declare no conflict of interest.

References

1. Leinonen, S. Exploration for Soapstone Occurrences: Use of Bulk Chemical Analyses to Select Potential Formation Areas. *Key Eng. Mater.* **2013**, *548*, 10–19. [CrossRef]
2. Selonen, O.; Pirinen, H.; Bulakh, A. Soapstone Production in Eastern Finland—A Historical Perspective. In *Geotechnical Report 12*; The Finnish Natural Stone Association: Helsinki, Finland, 2018; p. 39.
3. Niemelä, M. Talc-magnesite deposits in Finland. *Miner. Slov.* **2001**, *33*, 561–566.
4. Huhta, A.; Kärki, A. A proposal for the definition, nomenclature, and classification of soapstones. *GFF* **2018**, *140*, 38–43. [CrossRef]
5. Romanovich, I.F.; Satgaleev, Y.K.; Rakhmatulin, E.K. *Mineral Resources. Talc and Pyrophyllite*; Geoinformmark: Moscow, Russia, 1998; 38p.
6. Talc and Pyrophyllite. Statistics and Information. Available online: https://www.usgs.gov/centers/national-minerals-information-center/talc-and-pyrophyllite-statistics-and-information (accessed on 24 August 2023).
7. Talc, Soapstone and Steatite. *Indian Minerals Yearbook 2012*; (Part-III: Mineral Reviews); Indian Bureau of Mines: Nagpur, India, 2012; pp. 47-1–47-13.
8. Lehtinen, M.J. Chapter 9.5—Industrial Minerals and Rocks. In *Mineral Deposits of Finland*; Maier, W.D., Lahtinen, R., O'Brien, H., Eds.; Elsevier: Amsterdam, The Netherlands, 2015; pp. 685–710. [CrossRef]

9. Yehia, A.; Al-Wakeel, M.I. Talc separation from talc-carbonate ore to be suitable for different Industrial applications. *Miner. Eng.* **2000**, *13*, 111–116. [CrossRef]
10. Ann Bazar, J.; Rahimi, M.; Fathinia, S.; Jafari, M.; Chipakwe, V.; Chehreh Chelgani, S. Talc Flotation—An Overview. *Minerals* **2021**, *11*, 662. [CrossRef]
11. Luckeneder, C.; Gehringer, S.; Flachberger, H. Applicability of electrostatic separation on talc-containing mineral samples for production of a high-grade talc concentrate in comparison to flotation. *Berg Huettenmaenn. Monatsh.* **2022**, *167*, 381–385. [CrossRef]
12. Karlsen, T.A.; Rian, E.; Olesen, O. Overview of talc resources in the Altermark talc province, northern Norway, and possible uses of the talc ore. *Nor. Geol. Undersøkelse Bull.* **2000**, *436*, 93–102.
13. Spiridonov, T.M.; Zhernakov, V.; Baksheev, I.A.; Savina, D.N. Typomorphism of talc from apoultramafic metasomatites of the Urals. *Dokl. Akad. Nauk.* **2000**, *372*, 737–739.
14. Shand, M.A. *The Chemistry and Technology of Magnesia*; John Wiley & Sons: New York, NY, USA, 2006; p. 304. [CrossRef]
15. Hou, Q.; Luo, X.; Xie, Z.; Li, Y.; An, D.; Li, J. Preparation and characterization of microporous magnesia-based refractory. *Int. J. Appl. Ceram. Technol.* **2020**, *17*, 2629–2637. [CrossRef]
16. Alhaddad, M.S.; Ahmed, H.A.M. A Review of Magnesite Mineral and Its Industrial Application. *Arab. J. Sci. Publ.* **2022**, *2663*, 1–13.
17. Lamara, S.; Redaoui, D.; Sahnoune, F.; Heraiz, M.; Saheb, N. Microstructure, thermal expansion, hardness and thermodynamic parameters of cordierite materials synthesized from Algerian natural clay minerals and magnesia. *Bol. De La Soc. Esp. De Ceram. Y Vidr.* **2021**, *60*, 291–306. [CrossRef]
18. Gökçe, H.; Ağaoğulları, D.; Öveçoğlu, M.L.; Duman, İ.; Boyraz, T. Characterization of microstructural and thermal properties of steatite/cordierite ceramics prepared by using natural raw materials. *J. Eur. Cer. Soc.* **2011**, *31*, 2741–2747. [CrossRef]
19. de Almeida, E.P.; de Brito, I.P.; Ferreira, H.C.; de Lucena Lira, H.; de Lima Santana, L.N.; de Araújo Neves, G. Cordierite obtained from compositions containing kaolin waste, talc and magnesium oxide. *Cer. Int.* **2018**, *44*, 1719–1725. [CrossRef]
20. Valášková, M.; Zdrálková, J.; Simha Martynková, G.; Smetana, B.; Vlček, J.; Študentová, S. Structural variability of high purity cordierite/steatite ceramics sintered from mixtures with various vermiculites. *Cer. Int.* **2014**, *40*, 8489–8498. [CrossRef]
21. Yahya, A.; Soltan, A.; Mahani, R.; El-Kaliouby, B.; Kenawy, S.; Hamzawy, E.M.A. Electrical, microstructural and physical characteristics of talc-based cordierite ceramics. *Silicon* **2023**, *15*, 2901–2919. [CrossRef]
22. Storemyr, P.; Heldal, T. Soapstone Production through Norwegian History: Geology, Properties, Quarrying and Use. Asmosia 5—Interdisciplinary Studies on Ancient Stone. In Proceedings of the Fifth International Conference of the Association for the Study of Marble and Other Stones in Antiquity, Museum of Fine Arts, Boston, MA, USA, 11–15 June 1998; Herrman, J.J., Herz, N., Newman, R., Eds.; Archetype Publications: London, UK, 2002; pp. 359–369.
23. Vavro, M.; Gajda, J.; Přikryl, R.; Siegl, P. Soapstone as a locally used and limited sculptural material in remote area of Northern Moravia (Czech Republic). *Environ. Earth Sci.* **2015**, *73*, 4557–4571. [CrossRef]
24. Souza, H.N.; Reis, E.L.; Lima, R.M.F.; Cipriano, R.A.S. Using soapstone waste with diesel oil adsorbed as raw material for red ceramic products. *Ceram. Int.* **2016**, *42*, 16205–16211. [CrossRef]
25. Ferreira, W.L.; Reis, E.L.; Lima, R.M.F. Incorporation of residues from the minero-metallurgical industry in the production of clay-lime brick. *J. Clean. Prod.* **2015**, *87*, 505–510. [CrossRef]
26. Luukkonen, T.; Abdollahnejad, Z.; Yliniemi, J.; Mastali, M.; Kinnunen, P.; Illikainen, M. Alkali-activated soapstone waste—Mechanical properties, durability, and economic prospects. *Sustain. Mater. Technol.* **2019**, *22*, e00118. [CrossRef]
27. Sokolov, V.I. *Talc-Chlorite Schists and Their Application*; Karelian Research Centre, RAS: Petrozavodsk, Russia, 1995; 128p.
28. Dondi, M.; Raimondo, M.; Zanelli, C. Clays and bodies for ceramic tiles: Reappraisal and technological classification. *Appl. Clay Sci.* **2014**, *96*, 91–109. [CrossRef]
29. Doremus, R.H.; Duval, D.J.; Risbud, S.H.; Shackelford, J.F.; Bradt, R.C.; Wilding, M.C.; Davila, L.P.; Smith, J.D.; Fahrenholtz, W.G.; Velez, M.; et al. *Ceramic and Glass Materials. Structure, Properties and Processing*; Shackelford, G.F., Doremus, R.H., Eds.; Springer Science + Business Media, LLC: New York, NY, USA, 2008; 201p.
30. Semiz, B. Characteristics of clay-rich raw materials for ceramic applications in Denizli region (Western Anatolia). *Appl. Clay Sci.* **2017**, *137*, 83–93. [CrossRef]
31. Baumgart, W.; Dunham, A.C.; Amstutz, G.C. (Eds.) *Process Mineralogy of Ceramic Materials*; Ferdinand Enke Verlag: Stuttgart, Germany, 1984; 229p.
32. Avgustinik, A.I. *Ceramics*; Stroyizdat: Leningrad, USSR, 1975; 588p.
33. Dondi, M. Technological and Compositional Requirements of Clay Materials for Ceramic Tiles. In Proceedings of the 12th International Clay Conference, Bahía Blanca, Argentina, 22–28 July 2001; Elsevier: Amsterdam, The Netherlands, 2003; pp. 23–30.
34. Ismail, A.I.M.; Elmaghraby, M.S.; Shalaby, B.N.A. Flux ceramic tiles based on Egyptian trachyte. *Bull. Natl. Res. Cent.* **2022**, *46*, 226. [CrossRef]
35. Ilyina, V.P. Ceramic tile based on local hydromica clay and pegmatite tailings. *Glass Ceram.* **2022**, *79*, 12–19. [CrossRef]
36. Guryeva, V.A.; Prokofyeva, V.V. Building ceramics based on artificial serpentine as a raw material combined with low-grade clay. *Constr. Mater. Russ.* **2012**, *8*, 20–21.
37. Podkovyrov, V.N.; Maslov, A.V.; Kuznetsov, A.B.; Ershova, V.B. Lithostratigraphy and geochemistry of Upper Vendian—Lower Cambrian deposits in the Northeastern Baltic Monocline. *Stratigr. Geol. Correl.* **2017**, *25*, 1–20. [CrossRef]
38. Mitrofanova, Z.T.; Filintsev, G.P. *Karelia's Clays*; State Publishing House of the Karel. ASSR: Petrozavodsk, USSR, 1956; 158p.

39. Artamonov, V.S. *Karelia's Clays and Their Industrial Application*; State Publishing House of the Karelo-Finnish SSR: Petrozavodsk, USSR, 1950; 47p.
40. *Geological Map of the Russian Federation and Adjoining Water-Covered Areas. Scale 1:2500000*; Ministry of Natural Resources and Environment of the Russian Federation: Moscow, Russia; VSEGEI: Saint Petersburg, Russia, 2016.
41. Moore, D.M.; Reynolds, R.C. *X-ray Diffraction and the Identification and Analysis of Clay Minerals*, 2nd ed.; Oxford University Press: Oxford, NY, USA, 1997; 378p.
42. *ISO 17892-12:2018*; Geotechnical Investigation and Testing—Laboratory Testing of Soil—Part 12: Determination of Liquid and Plastic Limits. European Committee for Standardization: Brussels, Belgium, 2018.
43. *ISO 10545-2:2018*; Ceramic Tiles—Part 2: Determination of Dimensions and Surface Quality. European Committee for Standardization: Brussels, Belgium, 2018.
44. *ISO 10545-4:2019*; Ceramic Tiles—Part 4: Determination of Modulus of Rupture and Breaking Strength. European Committee for Standardization: Brussels, Belgium, 2019.
45. *ISO 10545-3:2018*; Ceramic Tiles—Part 3: Determination of Water Absorption, Apparent Porosity, Apparent Relative Density and Bulk Density. European Committee for Standardization: Brussels, Belgium, 2018.
46. Platunov, E.S. *Thermophysical Measurements in a Monotonic Regime*; Energy: Leningrad, Russia, 1973; 141p.
47. Baccour, N.A.; Koubaa, M.; Ben Jamaa, H.; Youssef, M.; Zuniga, M.A. A Comparative simulation study of link quality estimators in wireless sensor networks. In Proceedings of the IEEE International Symposium on Modeling, Analysis and Simulation of Computer and Telecommunication Systems, London, UK, 21–23 September 2009; pp. 1–10.
48. Casagrande, A. *Classification and Identification of Soils*; ASCE Trans.: Atlanta, GA, USA, 1947; pp. 901–991.
49. Carretero, M.I.; Dondi, M.; Fabbri, B.; Raimondo, M. The influence of shaping and firing technology on ceramic properties of calcareous and non-calcareous illitic–chloritic clays. *Appl. Clay Sci.* **2002**, *20*, 301–306. [CrossRef]
50. Ferrari, S.; Gualtieri, A.F. The use of illitic the production stoneware tile ceramics. *Appl. Clay Sci.* **2006**, *32*, 73–81. [CrossRef]
51. Sedmale, G.; Sperberga, I.; Sedmalis, U.; Valancius, Z. Formation of hightemperature crystalline phases in ceramic from illite clay and dolomite. *J. Eur. Ceram. Soc.* **2006**, *26*, 3351–3355. [CrossRef]
52. Wattanasiriwech, D.; Srijan, K.; Wattanasiriwech, S. Vitrification of illitic clay from Malaysia. *Appl. Clay Sci.* **2009**, *43*, 57–62. [CrossRef]
53. Dondi, M. Feldspathic fluxes for ceramics: Sources, production trends and technological value. *Resour. Conserv. Recycl.* **2018**, *133*, 191–200. [CrossRef]
54. Burkov, Y.K.; Vikulova, M.F.; Makedonov, A.V.; Tihomirova, N.Y.A.; Osipov, A.I.; Feofilova, A.P.; Kulokova, G.V.; Zemova, N.N. *Facies Types of Clayey Rocks (and Their Primary Lithological Characteristics)*; Nedra: Leningrad, Russia, 1973; 288p.
55. Wang, S.; Gainey, L.; Mackinnon, I.D.R.; Allen, C.; Gu, Y.; Xi, Y. Thermal behaviors of clay minerals as key components and additives for fired brick properties: A review. *J. Build. Eng.* **2023**, *66*, 105802. [CrossRef]
56. Wang, G.; Wang, H.; Zhang, N. In Situ high temperature X-ray diffraction study of illite. *Appl. Clay. Sci.* **2017**, *146*, 254–263. [CrossRef]
57. Ondro, T.; Hulan, T.; Al-Shantir, O.; Csaki, S.; Vaclavu, T.; Trnik, A. Kinetic analysis of the formation of high-temperature phases in an illite-based ceramic body using thermodilatometry. *J. Therm. Anal. Calorim.* **2019**, *138*, 2289–2294. [CrossRef]
58. Cheng, H.F.; Liu, Q.F.; Yang, J.; Ma, S.J.; Frost, R.L. The thermal behavior of kaolinite intercalation complexes-A review. *Thermochim. Acta* **2012**, *545*, 1–13. [CrossRef]
59. Gualteri, A.F.; Ferrari, S. Kinetics of illite dehydroxylation. *Phys. Chem. Miner.* **2006**, *33*, 490–501. [CrossRef]
60. Smykatz-Kloss, W.; Heide, K.; Klinke, W. Applications of Thermal Methods in the Geosciences. In *Handbook of Thermal Analysis and Calorimetry. Applications to Inorganic and Miscellaneous Materials*; Brown, M.E., Gallagher, P.K., Eds.; Elsevier: Amsterdam, The Netherlands, 2003; Volume 2, pp. 451–593.
61. Földvári, M. *Handbook of Thermogravimetric System of Minerals and Its Use in Geological Practice*; Geol. Inst. of Hungary: Budapest, Hungary, 2011; 180p.
62. Ptáček, P.; Šoukal, F.; Opravil, T.; Havlica, J.; Brandštetr, J. Crystallization of spinel phase from metakaoline: The nonisothermal thermodilatometric CRH study. *Powder Technol.* **2013**, *243*, 40–45. [CrossRef]
63. Steudel, A.; Kleeberg, R.; Koch, C.B.; Friedrich, F.; Emmerich, K. Thermal behavior of chlorites of the clinochlore-chamosite solid solution series: Oxidation of structural iron, hydrogen release and dihydroxylation. *Appl. Clay Sci.* **2016**, *132–133*, 626–634. [CrossRef]
64. Liu, X.W.; Liu, X.X.; Hu, Y.H. Investigation of the thermal decomposition of talc. *Clay Clay Miner.* **2014**, *62*, 137–144. [CrossRef]
65. Dondi, M.; Biasini, V.; Guarini, G.; Raimondo, M.; Argnani, A.; Di Primio, S. The influence of magnesium silicates on technological behaviour of porcelain stoneware tiles. *Key Eng. Mater.* **2001**, *206–213*, 1795–1798. [CrossRef]
66. Biasini, V.; Dondi, M.; Guarini, G.; Raimondo, M.; Argnani, A.; Di Primio, S. Effect of talc and chlorite on sintering and technological behavior of porcelain stoneware tiles. *Sil. Ind.* **2003**, *68*, 67–73.
67. *EN 14411:2016*; Ceramic Tiles—Definition, Classification, Characteristics, Assessment and Verification of Constancy of Performance and Marking. European Committee for Standardization: Brussels, Belgium, 2016.
68. Kingery, W.D.; Bowen, H.K.; Uhlmann, D.R. *Introduction to Ceramics*; Wiley: New York, NY, USA, 1976; 1032p.
69. El Ouahabi, M.; Daoudi, L.; Hatert, F.; Fagel, N. Modified Mineral Phases During Clay Ceramic Firing. *Clay Clay Miner.* **2015**, *63*, 404–413. [CrossRef]

70. Trindade, M.J.; Dias, M.I.; Coroado, J.; Rocha, F. Mineralogical transformations of calcareous-rich clays with firing: A comparative study between calcite and dolomiterichclays from Algarve, Portugal. *Appl. Clay Sci.* **2009**, *42*, 345–355. [CrossRef]
71. Trindade, M.J.; Dias, M.I.; Coroado, J.; Rocha, F. Firing tests on clay-rich raw materials from the Algarve Basin (southern Portugal): Study of mineral transformations with temperature. *Clay Clay Miner.* **2010**, *58*, 188–204. [CrossRef]
72. Dondi, M.; Ercolani, G.; Fabbri, B.; Marsigli, M. An approach to the chemistry of pyroxenes formed during the firing of Ca-rich silicate ceramics. *Clay Miner.* **1998**, *33*, 443–452. [CrossRef]
73. Orudzhev, F.M.; Ismajlova, M.A.; Avalova, E.V.; Mamedov, T.M.; Efendiev, M.E.I.; Lisov, F.M. Ceramic Mass for Manufacturing Facing Tile. SU. Patent 1211241, 15 February 1986.